Conflict Resolution Strategies for Balloon-Airship Encounters in Upper Class E Air Traffic Management (ETM)

Abraham K. Ishihara*
KBR, Moffett Field, CA, 94035

Min Xue†
NASA Ames Research Center, Moffett Field, CA, 94035

This paper examines strategic conflict resolution strategies for pair-wise high-altitude balloon, airship encounters. By strategic is meant that the conflict is identified (detected) at the time of flight plan submission or flight plan alteration through a service, such as an ETM Service Supplier (ESS). We investigate optimal control solutions for two classes of problems: non-cooperative, where the balloon must alter its ascent trajectory in order to avoid the airship and cooperative, where both vehicles make maneuvers through a negotiation protocol.

I. Introduction

With a projected market revenue of $4 billion by 2029 [1], High Altitude Platforms or HAPS operating in the stratospheric layer of the atmosphere have generated significant interest. The emergence of numerous commercial ventures coupled with an increasing presence of military missions will require new traffic management approaches in the stratospheric regimes. This is currently being investigated by NASA and the FAA and has been termed Upper Class E Airspace Traffic Management (ETM). As traditional approaches have focused on lower flight regimes with fixed-wing type vehicles, the properties of the stratosphere, in particular the significant variability in air density, temperature, and winds, coupled with a diverse set of vehicles including high-altitude balloons and airships motivate the need for new approaches to traffic management in this emerging space. A system modeled after UTM (UAS Traffic Management) [2**?**], where third parties can provide conflict management services is currently being investigated.

Lighter Than Air (LTA) Vehicles (airships, balloons, aerostats) are not new. However, the application of traditional airspace management concepts to these types of aircraft operations may have limited value for several reasons. For example, in the case of replacement of or augmentation to LEO (Low Earth Orbit) satellites for communication and internet coverage, swarms of LTA vehicles will likely be deployed in the form of a constellation. For example, the Google Loon project [3] leverages a network of super-pressurized balloons to provide internet coverage to rural regions. As new business models and objectives emerge, the number of potential encounters requiring conflict resolution may dramatically increase.

Given that the dynamics of LTA vehicles are vastly different than fixed wing aircraft operating in these altitude regimes, and that missions may be highly constrained by stratospheric winds and solar availability, new approaches to trajectory management are needed. The proposed approach presented in this paper could be utilized by third-party services to aid conflict management in support of ETM objectives by enabling real-time negotiation and optimal cost and trajectory computation. Numerous publications exist for conflict resolution between fixed-wing aircraft including distributed game-theoretic approaches[4, 5] where private information comprised of each indvidual cost functions and other internal data is hidden and only the pairs of trajectories and final costs or utilities are negotiated between agents. The approach presented here follows a similar framework by but focuses on LTA vehicle interaction where the dynamics, control, and optimal path generation are vastly different and also builds upon the UTM framework where the ESS plays a central role in flight plan submission, conformance and conflict resolution. Extensions of this work in a game-theoretic framework under various scenarios relevant to ETM airspace operations are currently being pursued by the authors.

The remainder of this paper is organized as follows. In Section II, we discuss the vehicle dynamics of the balloon and airship models. In Section III, we present the balloon optimal control problem formulation and discuss its numerical solution using the multiple shooting point method. In Section IV, we present our main results. Conclusions are presented in Section V.

*Chief Technical Advisor Engineering Systems, KBR, AIAA Member

†Aerospace Research Engineer, Aviation Systems Division, AIAA Senior Member

II. Vehicle Dynamics

Frames of reference shall be denoted by $\mathcal{F}_s$ and have associated with them three orthonormal vectors spanning the underlying vector space denoted by $\vec{i}^{(s)}$, $\vec{j}^{(s)}$, and $\vec{k}^{(s)}$. The axes of $\mathcal{F}_s$ shall be denoted by X_s, Y_s, and Z_s. A vector $\vec{r}$ with components (r_x, r_y, r_z) expressed in (or with respect to) frame $\mathcal{F}_s$ shall be written as $\vec{r}^{(s)} = r_x \vec{i}^{(s)} + r_y \vec{j}^{(s)} + r_z \vec{k}^{(s)} =: [r_x \; r_y \; r_z]_s^T$

Balloon Dynamics: Consider, in the inertial frame, $\mathcal{F}_e$, the velocity of point c located at the center of mass of the balloon. We may write $\vec{V}_c^{(e)} = \vec{V}_{rel}^{(e)} + \vec{W}^{(e)}$ where $\vec{V}_{rel}^{(e)}$ is the relative air velocity and $\vec{W}^{(e)}$, the wind field. Let $\vec{V}_c^{(e)} =: \left[\dot{x}_b^{(e)} \; \dot{y}_b^{(e)} \; \dot{z}_b^{(e)}\right]_e^T$ and $\vec{W}^{(e)} =: \left[\zeta_x^{(e)} \; \zeta_y^{(e)} \; \zeta_z^{(e)}\right]_e^T$. $\vec{V}_{rel}^{(e)}$ is thus given by $\vec{V}_{rel}^{(e)} = [\dot{x}_b^{(e)} - \zeta_x^{(e)} \; \dot{y}_b^{(e)} - \zeta_y^{(e)} \; \dot{z}_b^{(e)} - \zeta_z^{(e)}]_e^T$ Newton's second law yields

$$\begin{aligned} \vec{F}^{(e)} &= \vec{F}_{aero}^{(e)} + \vec{F}_{buoy}^{(e)} + \vec{F}_g^{(e)} \\ &= \frac{d}{dt}\left(m_b \vec{V}_{rel}^{(e)}\right) + \frac{d}{dt}\left(m_b \vec{W}^{(e)}\right) \end{aligned} \tag{1}$$

where m_b denotes the total mass of the balloon and $\vec{F}_{aero}^{(e)}$, $\vec{F}_{buoy}^{(e)}$, and $\vec{F}_g^{(e)}$ denote, respectively, the forces due to aerodynamics, buoyancy, and gravity. The aerodynamic force vector is given by

$$\vec{F}_{aero}^{(e)} = \frac{-\bar{q}_b S_b C_d}{\|\vec{V}_{rel}^{(e)}\|}\left((\dot{x}_b^{(e)} - \zeta_x^{(e)})\vec{i}^{(e)} + (\dot{y}_b^{(e)} - \zeta_y^{(e)})\vec{j}^{(e)} + (\dot{z}_b^{(e)} - \zeta_z^{(e)})\vec{k}^{(e)}\right) \tag{2}$$

where $\bar{q}_b = \frac{1}{2}\rho_a \|\vec{V}_{rel}^{(e)}\|^2$, S_b denotes a reference surface area, and C_d denotes the (non-dimensional) coefficient of drag. ρ_a denotes the ambient air density which depends on the altitude of the balloon [6, 7]. The buoyancy force is due to the mass of air that is displaced by the balloon and is given by $\vec{F}_{buoy}^{(e)} = m_a g \vec{k}^{(e)}$ where $m_a = \rho_a \frac{\pi}{6} d_b^3$ and d_b is the diameter of the balloon. The gravitational force is given by $\vec{F}_g^{(e)} = -m_b g \vec{k}^{(e)}$. where

$$m_b = m_{air}(t) + \rho_g \frac{\pi}{6} d_b^2 + \pi d_b^2 \mu_b + BOS_b = m_{air}(t) + m_0 \tag{3}$$

ρ_g denotes the density of the balloon's lifting gas (Helium), μ_b denotes the skin density, and BOS_b denotes the mass of all components other than the outer skin and lifting gas. $m_{air}(t)$ is the mass of internal air controlled by ballonets; it is time-varying and controlled via the equation $\dot{m}_{air}(t) = u(t) \in [-c_1, c_1]$ where $c_1 > 0$ denotes a maximum rate constant in units $[kg/s]$ determined by the ballonet pump motor. Using the ideal gas law, we have

$$p_a = \rho_a R_a T_a \quad \text{and} \quad p_g = \rho_g R_g T_g \tag{4}$$

where p_a is the ambient air pressure, R_a is the specific gas constant for air, T_a is the ambient air temperature, p_g is the internal pressure of the lifting gas, R_g is the specific gas constant of the lifting gas, and T_g is the internal temperature of the lifting gas. The specific gas constants may be computed by $R_s = \frac{\mathcal{R}}{\mathcal{M}_s}$ where $\mathcal{R} = 8.314$ [J/(mol K)] is the universal gas constant. Using $\mathcal{M}_a = 28.9647$ [g/mol] and $\mathcal{M}_g = 4$ [g/mol], we obtain $R_a = 297$ [J/(kg K)] and $R_g = 2080$ [J/(kg K)].

As mentioned above, the ambient air density term, ρ_a, can be computed from atmospheric data tables such as in [6, 7]. In order to compute ρ_g, we assume that $p_a = p_g$ and $T_a = T_g$. Using (4), we obtain $\rho_g = \rho_a \frac{R_a}{R_h}$. Lastly, we note that we need to account for a virtual mass term on the right hand side of (1). This term is not present in non-LTA dynamics since the mass of the air that is displaced by the vehicle is much smaller than the mass of the vehicle itself. We augment the right hand side of (1) as follows:

$$\vec{F}^{(e)} = \frac{d}{dt}\left((m_b + \eta m_a)\left(\vec{V}_{rel}^{(e)} + \vec{W}^{(e)}\right)\right) \tag{5}$$

Here the term η is a virtual mass factor term and is multiplied by the mass of the air displaced by the LTA vehicle. For a general ellipse, virtual mass equations have been derived [8] in the two directions as functions of eccentricity. Since a sphere is symmetric about all axes it is found that $\eta = 0.5$. Further explanation of virtual mass and virtual inertia for a general rigid body vehicle is discussed in the appendix.

Combining the equations above, and dropping the superscript '(e)' the balloon dynamics can be expressed as:

$$\begin{cases} \dot{x}_b = v_{bx} \\ \dot{y}_b = v_{by} \\ \dot{z}_b = v_{bz} \\ \dfrac{d}{dt}\left(\left(m_0 + m_{air}(t) + \eta m_a\right)\left(v_{bx} - \zeta_x\right)\right) = -\bar{q}_b S_b C_d \left(v_{bx} - \zeta_x\right) / \|\vec{V}_{rel}\| \\ \dfrac{d}{dt}\left(\left(m_0 + m_{air}(t) + \eta m_a\right)\left(v_{by} - \zeta_y\right)\right) = -\bar{q}_b S_b C_d \left(v_{by} - \zeta_y\right) / \|\vec{V}_{rel}\| \\ \dfrac{d}{dt}\left(\left(m_0 + m_{air}(t) + \eta m_a\right)\left(v_{bz} - \zeta_z\right)\right) = -\bar{q}_b S_b C_d \left(v_{bz} - \zeta_z\right) / \|\vec{V}_{rel}\| + (m_a - m_0 - m_{air}(t))g \\ \dot{m}_{air}(t) = u(t) \end{cases} \tag{6}$$

The airship dynamics are presented in the appendix. The parameters are taken primarily from reference [9] which models a YEZ-2A airship.

III. Optimal Control of Balloon

We begin by defining the optimal control problem that will be solved. Consider the following dynamical system to be controlled:

$$\begin{cases} \dot{x} = f(t, x, u) \\ x(t_0) = x_0 \end{cases} \tag{7}$$

defined on $t \in [t_0, t_f]$, where $f \in C(\mathbb{R}^+ \times \mathbb{R}^n \times \mathbb{R}^m; \mathbb{R}^n)$, $f_x \in C(\mathbb{R}^+ \times \mathbb{R}^n \times \mathbb{R}^m; \mathbb{R}^{n\times n})$ and u belongs to the space of left-piecewise continuous functions mapping $[t_0, t_f]$ into U where U is a closed and bounded subset of $\mathbb{R}^m$. Denote this space by $\mathcal{U} = C_p([t_0, t_f]; U)$. Let the cost function be given by

$$J[u] = \int_{t_0}^{t_f} L(s, x(s), u(s))ds + \phi(x(t_f)) \tag{8}$$

where L and ϕ denote, respectively, the running and terminal cost. We assume that L, L_x, ϕ, and ϕ_x are continuous with respect to their arguments. Let x_0 and x_f be two elements of the phase space associated with (7). The *optimal control problem*, in general*, is to find a $u \in \mathcal{U}$ which transfers the initial point x_0 to some final state x_f (provided that one such control exists) that, in addition, minimizes J. The pair $(x_0, u) \subset \mathbb{R}^n \times \mathcal{U}$ is said to be a feasible pair if the corresponding solution through (7) exists on the interval $[t_0, t_f]$. We denote this solution by $x(t; t_0, x_0, u)$.

Given the ordinary differential equation (ODE) in (7) and running cost in (8), we define the the Hamiltonian, $H : \mathbb{R}^+ \times \mathbb{R}^n \times \mathbb{R}^m \times \mathbb{R}^n \to \mathbb{R}$ by

$$H(t, x, u, p) \coloneqq p^T f(t, x, u) - L(t, x, u) \tag{9}$$

where p is the co-state and evolves according to

$$\begin{cases} \dot{p} = -\dfrac{\partial H}{\partial x} \\ p(t_f) = -\dfrac{\partial \phi(x(t_f))}{\partial x} \end{cases} \tag{10}$$

Throughout, if we do not explicitly state the arguments of H, it is assumed to be evaluated along the optimal trajectory. That is $H = H(t, x(t; t_0, x_0, u^*), u^*(t), p(t))$ where u^* is, assuming it exists, a control that locally optimizes the cost functional. The Pontryagin Maximum Principle (PMP) states that this control at each time $\tau \in (t_0, t_f]$ maximizes the Hamiltonian. That is,

$$H(\tau, x(\tau; t_0, x_0, u^*), u^*(\tau), p(\tau)) \geq H(\tau, x(\tau; t_0, x_0, u^*), v, p(\tau)) \tag{11}$$

*Numerous variants of this generic description exist including fixed final time, free final time, partially constrained final states, state constraints, etc.

for all $v \in U$. The maximization condition in (11) typically leads to an expression for the control, u. However, in order to compute it, both the plant dynamics in (7) and co-state dynamics in (10) must be evaluated. This typically requires numerically solving a Two-Point Boundary Value Problem (TPBVP) which can be quite challenging.

Balloon Optimal Control Law: Having described the optimal control problem and the approach we use to solve the corresponding TPBVP, we now apply it to the plant ODE described in (7). Consider only the z-component in (6) and with $\zeta_z = 0$.

$$\begin{cases} \dot{z}_b(t) = v_{bz}(t) \\ \dfrac{d}{dt}\left((M_v(z_b(t)) + m_{air}(t))v_{bz}(t)\right) = -\dfrac{1}{2}\rho_a(z_b(t))S_b C_d |v_{bz}(t)| v_{bz}(t) + (M_b(z_b(t)) - m_{air}(t))g \\ \dot{m}_{air}(t) = u(t) \\ z_b(t_0) = z_{b_z}^{(0)}; v_{b_z}(t_0) = v_{b_z}^{(0)}; m_{air}(t_0) = m_{air}^{(0)} \end{cases} \tag{12}$$

where $M_v(z_b(t)) \coloneqq m_0 + \eta m_a(z_b(t))$ and $M_b(z_b(t)) \coloneqq m_a(z_b(t)) - m_0$. Suppressing the explicit dependence on time, defining $x_1 = z_b$, $x_2 = v_{b_z}$, $x_3 = m_{air}$, and ignoring the time-derivative of the terms, $m_{air}(t)$ and M_v, that multiply vertical acceleration, (12) can be further simplified as follows:

$$\begin{cases} \dot{x}_1 = x_2 \\ \dot{x}_2 = \dfrac{1}{M_v(x_1) + x_3}\left((M_b(x_1) - x_3)g - \beta |x_2| x_2\right) \\ \dot{x}_3 = u \in [-c_1, c_1] \\ x_1(t_0) = x_{10}; x_2(t_0) = x_{20}; x_3(t_0) = x_{30} \end{cases} \tag{13}$$

where $x_{10} \coloneqq z_{b_z}^{(0)}$, $x_{20} \coloneqq v_{b_z}^{(0)}$, and $x_{30} \coloneqq m_{air}^{(0)}$. In our optimal control problem discussed below, we impose a final constraint on the balloon's terminal position and velocity as $x_1(t_f) = h_f$ and $x_2(t_f) = 0$. This represents the balloon ascending to a desired altitude and remaining there while minimizing a cost.

Non-Dimensionalization: Before we apply our optimal control machinery using (10) and (11), we non-dimensionalize (13). Non-dimensionalization is an important step in solving optimal control problems as it provides insight into the physics of the problem, ensures numerical robustness which is critical for highly sensitive schemes such as shooting methods, and provides a straightforward framework for perturbation analysis. To this end define a characteristic length, mass, and time as h_0, m_0, and $\hat{t}_f$, respectively, where h_0 is the distance from the initial to the final height (see Fig. 1.), m_0 is the non-ballonet balloon mass (see equation (3)), and $\hat{t}_f$ is the uncontrolled free ascent time to the terminal height[†]. $\hat{t}_f$ is determined numerically due to the presence of the nonlinear drag and time-varying air density terms. Define $\bar{x}_1 \coloneqq x_1/h_0$, $\tau \coloneqq t/\hat{t}_f$, and $\bar{x}_3 \coloneqq x_3/m_0$. Our non-dimensionalized plant dynamics become

$$\begin{cases} \bar{x}_1' = \bar{x}_2 \\ \bar{x}_2' = \dfrac{1}{\bar{M}_v + \bar{x}_3}\left((\bar{M}_b - \bar{x}_3)\bar{g} - \bar{\beta}|\bar{x}_2|\bar{x}_2\right) \\ \bar{x}_3' = \bar{u} \in [-\bar{c}_1, \bar{c}_1] \\ \bar{x}_1(\tau_0) = 0; \bar{x}_2(\tau_0) = \bar{v}_0; \bar{x}_3(\tau_0) = \bar{m}_{air}^{(0)} \end{cases} \tag{14}$$

where $\bar{M}_b \coloneqq M_b/m_0$, $\bar{M}_v \coloneqq M_v/m_0$, $\bar{g} \coloneqq \hat{t}_f^2 g/h_0$, $\bar{\beta} \coloneqq \beta h_0/m_0$, $\bar{u} \coloneqq \hat{t}_f u/m_0$, $\bar{m}_{air}^{(0)} \coloneqq m_{air}^{(0)}/m_0$, $\bar{v}_0 \coloneqq v_0/\hat{t}_f/h_0$, and $\bar{c}_1 \coloneqq c_1\hat{t}_f/m_0$. For the remainder we will take $\tau_0 = 0$. Additionally, for simplicity, we take the initial height of the balloon to be zero and translate air-density obtained from the MSISE tables [7] accordingly. The final results are then translated back to the actual initial height. Let us now define our cost functional to be minimized.

$$J[\bar{u}] \coloneqq \int_0^{\tau_f} (1-\gamma)|\bar{u}| + \gamma\bar{u}^2 + \alpha\bar{R}(\tau, \bar{x})ds \tag{15}$$

where $\gamma \in [0, 1]$ is a parameter that transitions the norm of $\bar{u}$ from L_1 to L_2 and α is a strength parameter for the repulsive field, $\bar{R}$ which is meant to resolve a conflict between the vehicles and is defined by $\bar{R} \coloneqq e^{-\frac{\|\bar{x}_a - \bar{x}\|^2}{2\bar{\mu}^2}}$ where $\bar{x}_a$

[†]The terminal height must be below the pressure altitude of the balloon otherwise solutions to the optimal control problem will not exist.

and $\bar{x}$ denote the position of the airship and balloon, respectively, and the parameters, α and $\bar{\mu}$, determine, respectfully, the strength and width of the repulsive field which can be tuned to provide a desired separation distance. The final (non-dimensionalized) time is defined to be $\tau_f := \inf\{s > 0 : \bar{x}_1(s) = 1 \text{ and } \bar{x}_2(s) = 0\}$.

The Hamiltonian (see Equation (9)) becomes

$$H = p_1\bar{x}_2 + p_3\bar{g}\left(\frac{\bar{M}_b - \bar{x}_3}{\bar{M}_v + \bar{x}_3}\right) - \frac{p_2\bar{\beta}\bar{x}_2^2}{\bar{M}_v + \bar{x}_3} + p_3\bar{u} - (1-\gamma)|\bar{u}| - \gamma\bar{u}^2 - \alpha\bar{R}(\tau, \bar{x}) \tag{16}$$

The co-state dynamics (see Equation (10)) become

$$\begin{cases} p_1' = -\dfrac{\alpha\bar{x}_1}{\bar{\mu}^2}\bar{R} \\ p_2' = -p_1 + \dfrac{2\bar{\beta}\bar{x}_2 p_2}{\bar{M}_v + \bar{x}_3} \\ p_3' = p_2\bar{g}\dfrac{\bar{M}_v + \bar{M}_b}{\left(\bar{M}_v + \bar{x}_3\right)^2} - \dfrac{p_2\bar{\beta}\bar{x}_2^2}{\left(\bar{M}_v + \bar{x}_3\right)^2} \\ p_1(0) = p_{10}; p_2(0) = p_{20}; p_3(0) = p_{30} \end{cases} \tag{17}$$

Our terminal conditions (again see Equation (10)) are $\bar{x}_1(\tau_f) = \bar{x}_2(\tau_f) = p_3(\tau_f) = 0$. Lastly, since τ_f is a free parameter to be optimized over, we have $H(\tau_f) = 0$ along the optimal trajectory. It (the Hamiltonian) is not, however, constant due to the repulsive term in the running cost which results in a time-varying running cost.

Multiple Shooting Point Method; In order to solve the optimal control problem, it is necessary to solve the ODE in (14), the co-state ODE in (17), and to choose $\bar{u}$ so as to maximize at each (non-dimensional) time step the Hamiltonian in (16). The primary obstruction to carrying this out is that the three initial co-states in (17) and the final time τ_f are, in general, unknown. Loosely speaking, the shooting point approach is when a guess of the unknown components[‡] of the initial state is made and the resulting Initial Value Problem (IVP) is then propagated forward in time via a numerical integration scheme such as Runga-Kutta 4th order (RK4). The resulting terminal values of the known components are then compared, and an error metric is used to modify the initial guess. Since analytical solutions to the TPBVP are generally not available, the process is treated as a black box, and numerical zero finding methods such as Newton-Raphson are typically employed. The problem, however, is the degree to which the terminal values are sensitive to changes in the initial conditions. The solution that is propagated, if it is stable, makes computation of the gradient difficult, if not impossible. This *hyper-sensitivity* motivates the need for alternative approaches such as the multiple shooting method [10, 11] where the time axis is divided into multiple segments. While this increases the number of unknowns that must be solved for, the interval of propagation is shortened minimizing the possibility of instability and reducing the sensitivity to changes. The MSM approach is employed to obtain the results presented in the next section.

IV. Results

Fig. 1 illustrates the main problem formulation. A balloon, initially at 18 km, is on an ascending trajectory to 20 km. An airship is headed laterally on an intersecting trajectory. The ESS (ETM service supplier which manages ETM operations including flight plan submission and conflict detection) has determined that a conflict exists and must resolve the conflict by considering maneuvers by both parties. Let J_a and J_b represent, respectfully, the cost functions of the airship and balloon, respectively. One possible approach to this problem is multi-objective optimization where a combination of J_a and J_b is optimized subject to the *combined* dynamic model constraints, control constraints and state constraints of the airship and balloon, respectively, are jointly optimized over the infinite dimensional control space. This, however, requires detailed information of the vehicle dynamics, constraints, cost functions, running costs, terminal costs, terminal constraints, etc., to be provided to the ESS in order to perform the joint optimization. Numerous issues can arise with this approach. First is scalability and real-time computation. Multi-agent optimal control is challenging computationally. While there exist solutions for pair-wise encounters, more than two agents can significantly increase computational cost and limit real-time applicability. Additionally, concerns regarding passing potentially proprietary performance data to an external party[§] may limit participation.

[‡]For many optimal control problems, the initial state of the plant to be controlled is known. We will assume this throughout.

[§]In the ESS framework, an operator is a client of an ESS which can be regarded as a service provider. From a organization perspective, an ESS is an external organization to the operator organization and any proprietary data required to be transferred between organizations may increase complexity and ultimately limit participation.

An alternative approach presented here allows each agent to compute its cost function for a finite number of possible trajectories. The cost functions are normalized and a simple negotiation protocol based on [12] is used to reach an agreement. We first discuss the uncooperative case.

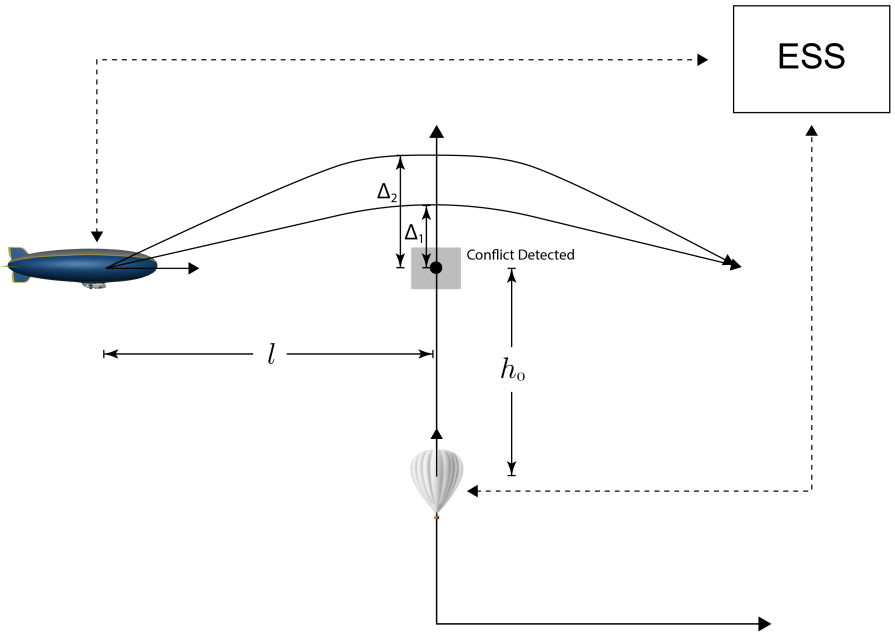

Fig. 1 LTA Vehicle Conflict

A. Uncooperative Case

In order to set up a conflict and pose its resolution, we must first generate two conflict trajectories. The airship's speed is determined by first considering the optimal balloon trajectory for the case when $\alpha = 0$ in (15). The optimal τ_f is determined for the balloon and is used to ensure there exists a conflict at the balloon's terminal position by choosing the magnitude of the airship's desired velocity to be $\bar{l}/\tau_f$ while it maintains a level (flight path angle of zero) flight path.

The following sequence of steps unfolds: The ESS in Fig. 1. determines that a conflict is to occur given the flight plans submitted by each vehicle. In the uncooperative case, we assume that only the balloon will be willing to modify its trajectory while the airship is uncooperative. The flight plan of the balloon is rejected by the ESS and the flight plan of the airship is conveyed by the ESS to the balloon operator in order to replan. We assume that given the flight plan, the balloon operator is able to generate an estimated airship trajectory consisting of position and velocity components at a suitable granularity[¶]. From the perspective of the balloon dynamical equations and cost function, the position and velocity of the airship can be treated as an exogenous term in the running cost repulsion term, $\bar{R}$. Given this information, the balloon computes an optimal collision-free trajectory using (14), (15), and (17).

In left sub-figure of Fig. 2, we show the resulting phase plots of the optimal trajectories for the case $\alpha = 0$ and $\alpha = 0.1$. Since the $\alpha = 0$ trajectory does not 'see' the oncoming airship, we observe that the balloon reaches a higher maximum velocity than the $\alpha = 0.1$ trajectory. With $\alpha = 0.1$, the maximum velocity is reduced as the balloon must travel slower in order to avoid the oncoming airship. In the right sub-figure of Fig. 2, we show the resulting non-dimensional phase-plots for $\alpha = 0.1$ at various stages of the MSM iteration. The weights that it is initialized with correspond to the $\alpha = 0$ case. Iterations for this case are not shown.

In the left sub-figure of Fig. 3, we plot the distance between the two vehicles as a function of time. In the $\alpha = 0$ case (red line), we see that the two vehicles indeed collide at the final time. In the $\alpha = 0.1$ case, we observe the vehicles maintain a minimum separation that exceeds $750[m]$. As stated before, this can be tuned by adjusting the $\bar{\mu}$ and α

[¶]Note that in the ETM concept, the operator is required to submit position updates to its corresponding ESS.

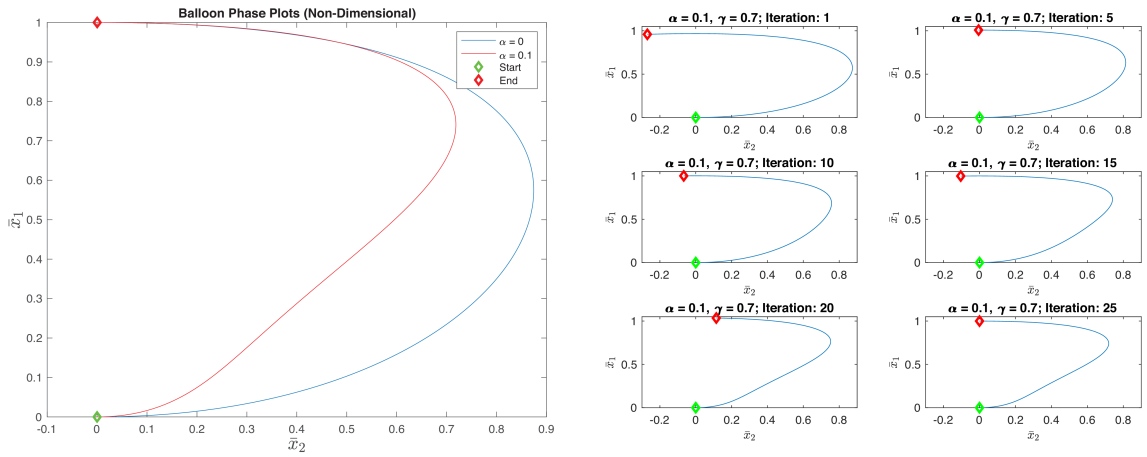

Fig. 2 Non-Dimensional Phase Plots

parameters. In the right sub-figure of Fig. 3., we plot the altitude as a function of time. We observe that the final time (the time that it reaches the terminal condition) in the $\alpha = 0.1$ case is indeed larger than in the $\alpha = 0$ case. We also plot the total cost for both cases. This was accomplished by appending a fictitious state whose derivative is set equal to the running cost in (15). We observe that the $\alpha = 0.1$ case results in a higher running cost which can be attributed to a longer trajectory flight time (τ_f) due to the need to avoid colliding with the airship.

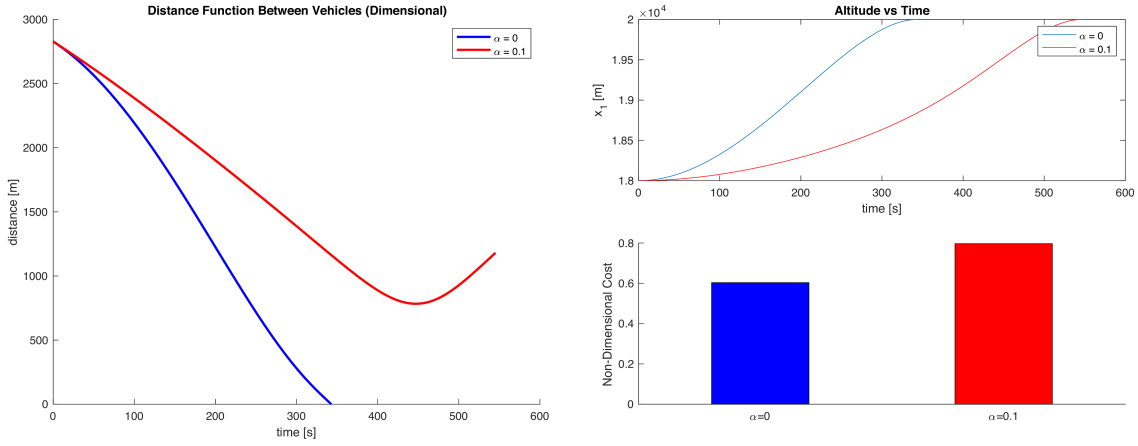

Fig. 3 Distance, $\bar{x}$-trajectory, and Cost

B. Cooperative Case

In this scenario, the airship participates in the process by engaging in a negotiation process with the balloon facilitated by the ESS. In order to decribe the process which is based on the frameworks proposed in [4, 5], we need several definitions. The negotiation proceeds iteratively where at each iteration, each agent proposes a deal to the other agent. Let $T_i^{(s)}$ denote the ith trajectory proposed by agent $s \in \{a, b\}$. Let $R^{(\bar{s})}(T_i^{(s)})$ denote the response trajectory of agent $\bar{s}$ to agent s's proposed trajectory, $T_i^{(s)}$, where

$$\bar{s} = \begin{cases} a & \text{if } s = b \\ b & \text{if } s = a \end{cases}$$

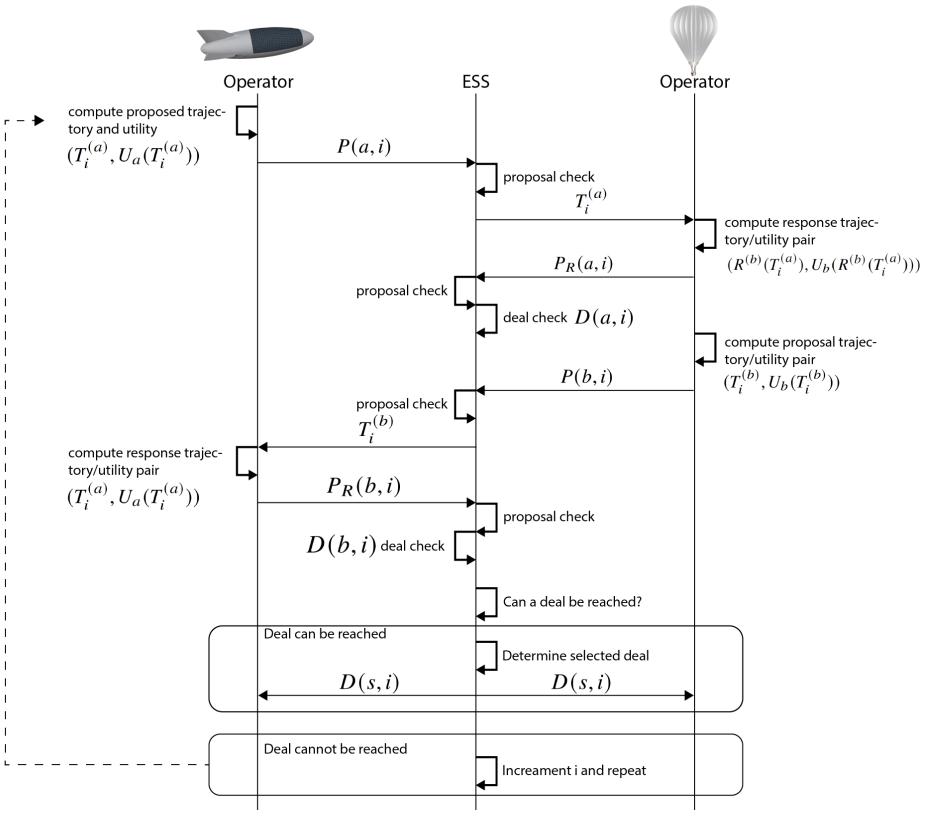

Fig. 4 Sequence Diagram

We assume that $T_i^{(s)}$ and $R^{(\bar{s})}(T_i^{(s)})$ belong to the appropriate (infinite dimensional) function space (for example the solution space associated with the ODE in (6)) and its transmission to an ESS is accomplised by a truncation to a sequence of four dimensional way-points with sufficient granularity that would enable another vehicle to use the information to generate a conflict-free trajectory. Corresponding to each proposed trajectory, $T_i^{(s)}$, is an associated proposed trajectory cost, $C^{(s)}(T_i^{(s)})$, and to each response trajectory, $R^{(\bar{s})}(T_i^{(s)})$, a corresponding response trajectory cost, $C^{(\bar{s})}(R^{(\bar{s})}(T_i^{(s)})$. Note that we use the term $C^{(s)}$ instead of J (see equation (8)) since we want to emphasize the dependence on the trajectory which directly impacts the response trajectory. The argument of $J[\cdot]$ is a control which ultimately generates a trajectory.

Let us assume that each agent has a finite set of N trajectories from which to construct deals (defined subsequently below). Define them by $\mathcal{T}^{(a)} = \{T_1^{(a)}, T_2^{(a)}, \ldots, T_N^{(a)}\}$ and $\mathcal{T}^{(b)} = \{T_1^{(b)}, T_2^{(b)}, \ldots, T_N^{(b)}\}$. Further assume they are ordered and their associated costs normalized such that

$$\begin{aligned} &C^{(s)}(T_i^{(s)}) \leq C^{(s)}(T_{i+1}^{(s)}) \quad i \in [1, N-1] \\ &C^{(s)}(T_1^{(s)}) = 0 \ \text{ and } \ C^{(s)}(T_N^{(s)}) = 1 \end{aligned} \tag{18}$$

For all definition that follow, we assume $s \in \{a, b\}$ and $i \in [1, N]$ unless otherwise stated.

Definition IV.1 (Deal)**.** *A* deal*, $D(s,i)$, proposed by agent s at iteration i is a pair $(T_i^{(s)}, R^{(\bar{s})}(T_i^{(s)}))$.*

Definition IV.2 (Utility)**.** *Let $D(s,i)$ denote a deal proposed by agent s at iteration i. Then, the utility of deal $D(s,i)$ for agent s is defined to be $U_s(D(s,i)) := 1 - C^{(s)}(T_i^{(s)}) \in [0,1]$. The utility of deal $D(s,i)$ for agent $\bar{s}$ is defined to be $U_{\bar{s}}(D(s,i)) := 1 - C^{(\bar{s})}(R^{(\bar{s})}(T_i^{(s)})) \in [0,1]$*

Definition IV.3 (Rational Deal, Parato Optimality, Negotiation Set, and Conflict Deal)**.** *A deal $D(s,i)$ is said to be* rational *if $U_s(D(s,i))$ and $U_{\bar{s}}(D(s,i))$ are non-negative. A deal, D, is said to* dominate *another deal, D', if*

$$\begin{aligned} &U_a(D) \geq U_a(D') \text{ and } U_b(D) > U_b(D') \text{ or} \\ &U_a(D) > U_a(D') \text{ and } U_b(D) \geq U_b(D') \end{aligned}$$

A deal is said to be pareto *optimal if it is not dominated by any other deal. The set of all individually rational and pareto optimal deals comprise the* Negotiation Set *(NS). Lastly, we define the conflict deal $\bar{D} = (T_N^{(a)}, T_N^{(b)})$. This is the deal that results if no agreement is reached. It results in the worst case cost for both agents.*

Remark 1. *Note that the utility for agent s of deal $D(s,i)$ depends only on agent s's proposed trajectory $T_i^{(s)}$ and not the response trajectory. Hence we may write $U_s(D(s,i)) = U_s(T_i^{(s)})$. D dominates D' if the deal improves the utility of at least one agent and does not harm any others. The equivalent of condition (18) using utilities is*

$$\begin{aligned} &U_s(T_i^{(s)}) \geq U_s(T_{i+1}^{(s)}) \quad i \in [1, N-1] \\ &U_s(T_1^{(s)}) = 1 \;\; \textit{and} \;\; U_s(T_N^{(s)}) = 0 \end{aligned} \tag{19}$$

We will use, in this rendition, the ESS to not only facilitate inter-agent communication, but also to serve as an arbiter that checks proposals (defined next) and deals as they evolve throughout the negotiation phase. In addition, once an agreement has been reached (even if it is the conflict agreement), the ESS will convey to each agent (and enforce to the extent it can and does currently for non-conflicting flight plans) the agreement trajectory that it is required to be implemented and flown. We do not, in this paper, discuss the specific communication protocols (for example HTTP or websocket), nor how identity, authentication, and authorization whether centralized or decentralized is to be implemented. In order to further discuss the role of the ESS in negotiation, we need the following two definitions.

Definition IV.4 (Proposal)**.** *Define a proposal, $P(s,i)$, associated with deal $D(s,i)$ to be the pair $(T_i^{(s)}, U_s(T_i^{(s)}))$ that agent s transmits to the ESS (see Fig. 4. below). Define a response proposal, $R_P(s,i)$, associated with deal $D(s,i)$ to be the pair $(R^{(\bar{s})}(T_i^{(s)}), U_{\bar{s}}(T_i^{(s)}))$.*

In order to facillitate the selection of a deal in the case where both proposals are acceptable, we need the following:

Definition IV.5 (Product Utility)**.** *The product utility of a deal is defined by*

$$\Pi(D(s,i)) = U_s(T_i^{(s)}) \cdot U_{\bar{s}}(R^{(\bar{s})}(T_i^{(s)}))$$

Negotiation Protocol: As mentioned above, agents incrementally propose and counter-propose to one another until a deal is agreed upon. We now describe this in detail. An iteration begins with agent a computing a proposed trajectory, $T_i^{(a)}$, and its associated utility $U_a(T_i^{(a)})$. It then transmits proposal $P(s,i)$ to the ESS[‖]. The ESS then checks the proposal to ensure its validity. But this is meant checking condition (19) and the validity of proposed trajectory $T_i^{(a)}$**. The ESS then transmits the trajectory $T_i^{(a)}$ to agent b who then computes a response trajectory, $R^{(b)}(T_i^{(a)})$, and its corresponding utility, $U_b(R^{(b)}(T_i^{(a)}))$. Agent b transmits the response propose $P_R(a,i)$ to the ESS where it is validated. The deal, $D(a,i)$ is now determined, and the ESS checks its (the deal's) validity[††]. This process is then repeated for agent b concluding with the validation of $D(b,i)$.

The ESS must now determine if a deal can be agreed to or not. First, the conflict deal is checked (see Definition IV.3). This is the case where both agents decide simultaneously (within the same iteration) to forgo any concession to the other. If this occurs, negotiation concludes and the ESS informs the agents and accepts the highest cost trajectories (lowest utility) as the resolution. If this does not occur, the ESS then checks if a deal can be reached. Define

$$G(s,i) \coloneqq U_{\bar{s}}(R^{(\bar{s})}(T_i^{(s)})) - U_{\bar{s}}(T_i^{(\bar{s})}) \tag{20}$$

[‖] In general, both agents may simultaneously initiate proposals to the ESS; it need not be in any particular order.

** Given a flight plan submission to an ESS, the ESS must ensure it is conflict free with respect to all of its own operations (intra-ESS) and all other operations (inter-ESS). Details of the current state of this work and its implementation leveraging DSS is beyond the scope of the present paper.

[††] Validity of a deal could including checking minimum separation and other safety criteria.

$G(s,i) \geq 0$ implies that agent $\bar{s}$ is willing to accept agent s's deal. $G(s,i) < 0$ implies that agent $\bar{s}$ is not willing to accept agent s's deal. Hence, to determine if a deal *can* be reached, there must exist an $s \in \{a,b\}$ such that $G(s,i) \geq 0$. If this is not true, we conclude negotiation for round i and repeat for the next round $i+1$. If it is true, the ESS selects a deal as follows: If $G(a,i) \geq 0$ and $G(b,i) < 0$, deal $D(a,i)$ is selected. If $G(b,i) \geq 0$ and $G(a,i) < 0$, deal $D(b,i)$ is selected. If $G(a,i) \geq 0$ and $G(b,i) \geq 0$, we compute $s^* := \arg\max_{s\in\{a,b\}} \Pi(D(s,i))$. If s^* is unique, then the deal selected is $D(s^*,i)$. If not, a coin toss determines the deal. This concludes our description of the negotiation process and is depicted in Fig. 4. By Theorem 3 in [12] it must converge in finite time. We do not in this paper discuss strategies that can be played by each agent.

In this particular example, the airship selects $P = 7$ trajectories with trajectory i corresponding to a $\Delta_i = (i-1)\Delta_0$ where $\Delta_0 = 300$ [m]. Δ_i is the maximal height above 2000 [km] that the airship reaches at the origin (see Fig. 1). In the left sub-figure of Fig. 5., to each airship trajectory, $T_i^{(a)}$ for $i \in [1,7]$, proposed, we plot the corresponding balloon optimal trajectory, $T_i^{(b)}$ for $i \in [1,7]$, as a phase plot. In the right sub-figure of Fig. 5., we plot the corresponding normalized response costs, $C_i^{(b)}$ for $i \in [1,7]$. The highest cost is equal to 1 and corresponds to the uncooperative case discussed in Subsection IV.A above where the airship does not make any compensatory maneuvers (compare to Fig. 2). Fig. 6. depicts the utilities during the negotiation sequence until its convergence at step 4.

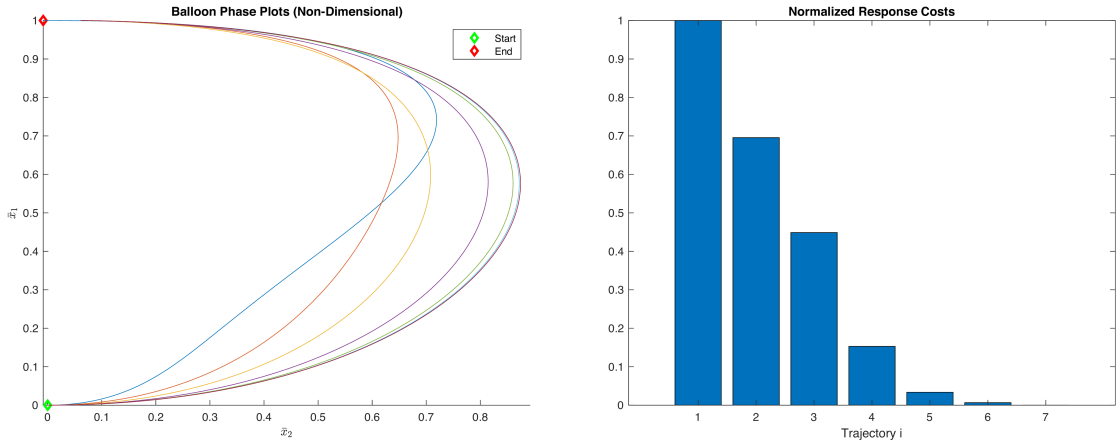

Fig. 5 Balloon Phase Plots and Normalized Response Costs.

iteration	airship proposed utility	balloon response utility	balloon proposed utility	airship response utility
1	1.00	0.00	1.00	0.00
2	0.83	0.30	0.83	0.47
3	0.67	0.55	0.67	0.62
4	0.50	0.85	0.50	0.73

Fig. 6 Negotiation Iteration

V. Conclusion

This paper examined strategic conflict avoidance strategies for pair-wise high-altitude balloon-airship encounters. An approach where only individual trajectories and normalized cost functions are transmitted to an ESS is proposed. Balloon optimal trajectories were examined and solved for using the Multiple Shooting Method (MSM). Associated costs corresponding to airship trajectories were computed. The proposed approach could be used by ESSs to facilitate negotiation and conflict resolution in the upper Class E airspace.

A. Airship Dynamics

Consider Fig. 7. It is typical in the modeling and control of fixed-wing aircraft to define the origin of the body-fixed

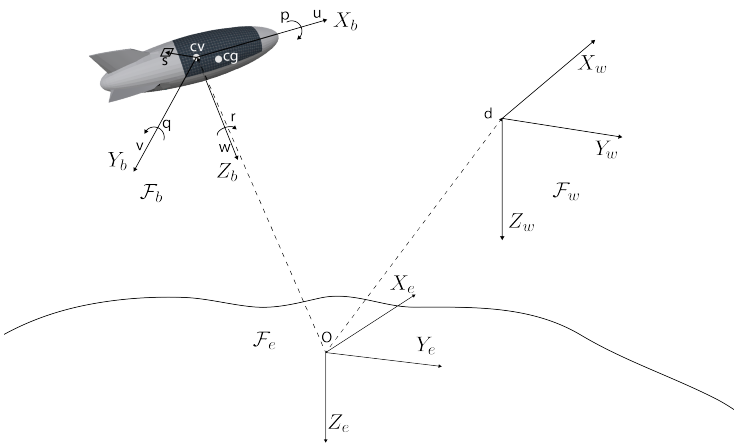

Fig. 7 Airship Reference Frames

axis at the center of gravity of the vehicle. This results in a significant simplification of the equations of motion by exploiting the fact that $\int_{\mathcal{V}} \rho(x,y,z)\left(\vec{r}_s^{(e)} - \vec{r}_c^{(e)}\right) dV = 0$ where $\vec{r}_c^{(e)}$ denotes the center of gravity and $\rho(x,y,z)$ denotes the density of the vehicle at point (x,y,z). However, in modeling and control of airships, it is not advantageous to do so. The two reason are that the buoyant force acts through the center of volume and that the position of the center of gravity (CG) changes over time due to the ballonets. It is for this reason that the body-fixed axis is located at the center of volume as depicted in Fig. 7. We need some preliminary definitions: Let the body frame of the airship rotate with angular rate vector $\vec{\omega}^{(b)} = [p\ q\ r]^T$ and let $\vec{v}^{(b)} \coloneqq [u\ v\ w]^T$ denote the relative body fixed velocity vector. Let wind vector with respect to the body frame (also see balloon dynamics section) be defined by $\vec{W}^{(b)} = [\zeta_x^{(b)}\ \zeta_y^{(b)}\ \zeta_z^{(b)}]^T$ and define[‡‡] $\vec{v}_\zeta^{(b)} \coloneqq [u+\zeta_x^{(b)}\ v+\zeta_y^{(b)}\ w+\zeta_z^{(b)}]^T$. Let the position of the CG in the body-fixed reference frame, $\mathcal{F}_b$ be given by $\vec{r}_{cg}^{(b)} = [d_x\ d_y\ d_z]_b^T$. Accounting for the non-zero term $\int_V \rho\, \vec{r}_{sc}^{(e)}\, dV = m\, \vec{r}_{cg,c}^{(e)}$, where m is the total mass of the airship, the force and moment equations may be compactly expressed as

$$\begin{bmatrix} mI_{3\times3} & mD_{cg} \\ -mD_{cg} & I \end{bmatrix} \begin{bmatrix} \dot{\vec{v}}_\zeta^{(b)} \\ \dot{\vec{\omega}}^{(b)} \end{bmatrix} + \begin{bmatrix} \vec{H}_F \\ \vec{H}_M \end{bmatrix} + m \begin{bmatrix} \vec{A}_{cg} \\ \vec{B}_{cg} \end{bmatrix} = \begin{bmatrix} \vec{F}^{(b)} \\ \vec{M}^{(b)} \end{bmatrix} \tag{21}$$

where

$$D_{cg} = \begin{bmatrix} 0 & d_z & -d_y \\ -d_z & 0 & d_x \\ d_y & -d_x & 0 \end{bmatrix} \qquad \vec{H}_F = m\vec{\omega}^{(b)} \times \vec{v}_\zeta^{(b)} \qquad \vec{H}_M = \vec{\omega}^{(b)} \times I\vec{\omega}^{(b)} \tag{22}$$

and

$$\vec{A}_{cg} = \begin{bmatrix} -d_x(q^2+r^2) + d_y pq + d_z pr \\ -d_y(p^2+r^2) + d_z rq d_x pq \\ -d_z(p^2+q^2) + d_x pr + d_y qr \end{bmatrix} \qquad \vec{B}_{cg} = \begin{bmatrix} d_y\left(pv_\zeta - qu_\zeta\right) - d_z\left(ru_\zeta - pw_\zeta\right) \\ d_z\left(qw_\zeta - rv_\zeta\right) - d_x\left(pv_\zeta - qu_\zeta\right) \\ d_x\left(ru_\zeta - pw_\zeta\right) - d_y\left(qw_\zeta - rv_\zeta\right) \end{bmatrix} \tag{23}$$

$\vec{F}^{(b)} = \vec{F}_p^{(b)} + \vec{F}_a^{(b)} + \vec{F}_g^{(b)} + \vec{F}_{buoy}^{(b)}$ where $\vec{F}_p^{(b)}$, $\vec{F}_a^{(b)}$, $\vec{F}_g^{(b)}$, and $\vec{F}_{buoy}^{(b)}$ denote, respectively, forces due to propulsion, aerodynamics, gravity and buoyancy. Since gravity and buoyancy forces are parallel (in the inertial reference frame)

[‡‡] $\vec{\omega}^{(b)}$ should also acquire a rotational wind component but we assume it be negligible.

to $\vec{k}^{(e)}$, we may combine them as $\vec{F}_{bg}^{(e)} \coloneqq [0\ 0\ \tilde{m}g]_e^T$ where $\tilde{m} \coloneqq m - m_a$. $m_a = \rho \cdot Vol$ denotes the mass of the air displaced by the airship. We have not, in Equation (21), accounted for angular monmentum terms arising from spinning rotors. These terms would need to be included in $\vec{H}_M$. The external moment is given by $\vec{M}^{(b)} = \vec{M}_p^{(b)} + \vec{M}_a^{(b)} + \vec{M}_g^{(b)}$ which denotes the moment contributions arising from propulsion, aerodynamics, and gravity[§§]

Virtual Mass and Inertia: Additional complications arise when modeling airships (or LTA vehicles in general). Consider the airship in Fig. 7 moving along its desired trajectory. As it accelerates, it induces a motion in the surrounding fluid particles that would otherwise remain stationary had the vehicle not moved at all. The fluid particles are pushed aside and then close behind the vehicle acquiring a kinetic energy that would otherwise not have been present. This acquistion of kinetic energy by the fluid is accomplished by work (force acting through a displacement) done on the fluid. The force, in this case, arises from the pressure that the airship exerts as it moves, and by virtue of Newton's third law, the fluid, therefore, exerts a force on the airship of equal magnitude and in opposite direction. This fact is what we must account for on the right hand sides of Equation (21).

To this end, we augment[¶¶] (additively) the terms $\vec{F}^{(b)}$ and $\vec{M}^{(b)}$ by, respectively, $\vec{F}_v^{(b)}$ and $\vec{M}_v^{(b)}$. They are given by

$$\vec{F}_v^{(b)} = \Gamma_1 \dot{\vec{\nu}} + \Gamma_2 \dot{\vec{\omega}} + E_F \qquad\qquad \vec{M}_v^{(b)} = \Gamma_3 \dot{\vec{\nu}} + \Gamma_4 \dot{\vec{\omega}} + E_M \tag{24}$$

where

$$\Gamma_1 = \begin{bmatrix} X_{\dot{u}} & X_{\dot{v}} & X_{\dot{w}} \\ X_{\dot{v}} & Y_{\dot{v}} & Y_{\dot{w}} \\ X_{\dot{w}} & Y_{\dot{w}} & Z_{\dot{w}} \end{bmatrix} \qquad \Gamma_2 = \begin{bmatrix} X_{\dot{u}} & X_{\dot{v}} & X_{\dot{w}} \\ X_{\dot{v}} & Y_{\dot{v}} & Y_{\dot{w}} \\ X_{\dot{w}} & Y_{\dot{w}} & Z_{\dot{w}} \end{bmatrix} \qquad E_F = \begin{bmatrix} E_x \\ E_y \\ E_z \end{bmatrix} \tag{25}$$

where

$$\begin{aligned} E_x &= Z_{\dot{w}} qw + Z_{\dot{q}} q^2 + X_{\dot{w}} qu - Y_{\dot{v}} rv - Y_{\dot{p}} rp - Y_{\dot{r}} r^2 - X_{\dot{v}} ru - Y_{\dot{w}} rw - (Y_{\dot{q}} - Z_{\dot{r}}) rq \\ E_y &= X_{\dot{v}} rv - Y_{\dot{w}} pv - Z_{\dot{p}} p^2 + X_{\dot{r}} r^2 + (X_{\dot{p}} - Z_{\dot{r}}) pr - X_{\dot{w}} pu + X_{\dot{w}} rw - Z_{\dot{w}} pw + X_{\dot{u}} ru - Z_{\dot{q}} pq + X_{\dot{q}} rq \\ E_z &= -X_{\dot{w}} qw - X_{\dot{u}} qu - X_{\dot{q}} q^2 + Y_{\dot{v}} pv + Y_{\dot{r}} rp + Y_{\dot{p}} p^2 + Y_{\dot{w}} pw + X_{\dot{v}} pu - X_{\dot{v}} qv - (X_{\dot{p}} - Y_{\dot{q}}) pq - X_{\dot{r}} qr \end{aligned} \tag{26}$$

The constants that appear in (25), for example $X_{\dot{u}}$, represent the rate of change of a force with respect to an acceleration. Assuming that airship can be modeled as a *finless*[***] *prolated spheriod*, massive simplifications to (25) and (26) occur. Specifically, this assumption results in:

$$X_{\dot{v}} = X_{\dot{w}} = X_{\dot{p}} = X_{\dot{q}} = X_{\dot{r}} = Y_{\dot{w}} = Y_{\dot{p}} = Y_{\dot{q}} = Y_{\dot{r}} = Z_{\dot{p}} = Z_{\dot{q}} = Z_{\dot{r}} = K_{\dot{p}} = K_{\dot{q}} = K_{\dot{r}} = M_{\dot{r}} = 0 \tag{27}$$

For the non-zero virtual acceleration derivatives in (26), and masses, inertias, and aerodynamic coefficients in (21), we utilize the data provided in reference [14]. We omit, due to page limitations, further details of the model and the derivation of the control law used in the tracking of the trajectories that generated Fig. 3. and Fig. 5. Details will be provided in a follow on publication.

References

[1] "NSR Report: HAPs Market to Generate $4 Billion by 2029," `https://www.nsr.com/nsr-report-haps-market-to-generate-4-billion-by-2029/`, 2020.

[2] Aweiss, A., Homola, J., Rios, J., Jung, J., Johnson, M., Mercer, J., Modi, H., Torres, E., and Ishihara, A., "Flight Demonstration of Unmanned Aircraft System (UAS) Traffic Management (UTM) at Technical Capability Level 3," *2019 IEEE/AIAA 38th Digital Avionics Systems Conference (DASC)*, 2019, pp. 1–7. https://doi.org/10.1109/DASC43569.2019.9081718.

[3] Nagpal, L., and Samdani, K., "Project Loon: Innovating the connectivity worldwide," *2017 2nd IEEE International Conference on Recent Trends in Electronics, Information & Communication Technology (RTEICT)*, IEEE, 2017, pp. 1778–1784.

[§§] The gravitational force acts through the center of gravity which causes a moment about the center of volume which is the origin of the body-axis reference frame.

[¶¶] The deriviation of the forces and moments that arise from the presure exerted on it by the surrounding fluid can be accomplised by considering the total kinetic energy of the fluid which is derived in [13] on page 163. Using the expression for kinetic energy, the forces and moments can be derived by Kirchoff's equations.

[***] This assumption implies that there is no dorsal fin nor symmetric fins in the rear of the vehicle.

[4] Wollkind, S., Valasek, J., and Ioerger, T., "Automated conflict resolution for air traffic management using cooperative multiagent negotiation," *AIAA Guidance, Navigation, and Control Conference and Exhibit*, 2004, p. 4992.

[5] Pritchett, A. R., and Genton, A., "Negotiated decentralized aircraft conflict resolution," *IEEE transactions on intelligent transportation systems*, Vol. 19, No. 1, 2017, pp. 81–91.

[6] Minzner, R., "The 1976 standard atmosphere and its relationship to earlier standards," *Reviews of geophysics*, Vol. 15, No. 3, 1977, pp. 375–384.

[7] Picone, J., Hedin, A., Drob, D. P., and Aikin, A., "NRLMSISE-00 empirical model of the atmosphere: Statistical comparisons and scientific issues," *Journal of Geophysical Research: Space Physics*, Vol. 107, No. A12, 2002, pp. SIA–15.

[8] Lamb, H., "The inertia coefficients of an ellipsoid moving in fluid," *Advisory Committee for Aeronautics, Reports and Memoranda No. 623, London, UK*, 1918.

[9] Gomes, S. B. V., and Ramos, J. G., "Airship dynamic modeling for autonomous operation," *Proceedings. 1998 IEEE International Conference on Robotics and Automation (Cat. No. 98CH36146)*, Vol. 4, IEEE, 1998, pp. 3462–3467.

[10] Bulirsch, R., Stoer, J., and Stoer, J., *Introduction to numerical analysis*, Vol. 3, Springer, 2002.

[11] Keller, H. B., *Numerical methods for two-point boundary-value problems*, Courier Dover Publications, 2018.

[12] Zlotkin, G., and Rosenschein, J. S., "Negotiation and Task Sharing Among Autonomous Agents in Cooperative Domains." *IJCAI*, Vol. 89, Citeseer, 1989, pp. 20–25.

[13] Lamb, H., *Hydrodynamics*, University Press, 1924.

[14] Gomes, S., "An investigation into the flight dynamics of airships with application to the YEZ-2A," Ph.D. thesis, Cranfield University, 1990.